Crystal structure of encorafenib, $C_{22}H_{27}ClFN_7O_4S$

James A. Kaduk,[1,2,a] Anja Vieira Dosen,[3] and Thomas N. Blanton[3]
[1]*Illinois Institute of Technology, 3101 S. Dearborn St., Chicago, IL 60616, USA*
[2]*North Central College, 131 S. Loomis St., Naperville, IL 60540, USA*
[3]*ICDD, 12 Campus Blvd., Newtown Square, PA 19073-3273, USA*

(Received 24 November 2022; accepted 21 February 2023)

The crystal structure of encorafenib, $C_{22}H_{27}ClFN_7O_4S$, has been solved and refined using synchrotron X-ray powder diffraction data, and optimized using density functional theory techniques. Encorafenib crystallizes in space group $P2_1$ (#4) with $a = 16.17355(25)$, $b = 9.52334(11)$, $c = 17.12368(19)$ Å, $\beta = 89.9928(22)°$, $V = 2637.50(4)$ Å^3, and $Z = 4$. The crystal structure consists of alternating layers of stacked halogenated phenyl rings and the other parts of the molecules perpendicular to the *a*-axis. One molecule participates in two strong N–H···N hydrogen bonds (one intra- and the other intermolecular), which are not present for the other molecule. The intermolecular hydrogen bonds link molecule 2 into a spiral chain along the *b*-axis. The powder pattern has been submitted to ICDD for inclusion in the Powder Diffraction File™ (PDF®).

[doi:10.1017/S0885715623000118]

Key words: encorafenib, Braftovi, crystal structure, Rietveld refinement, density functional theory

I. INTRODUCTION

Encorafenib ($C_{22}H_{27}ClFN_7O_4S$, sold under the brand name BRAFTOVI) is a kinase inhibitor. Encorafenib inhibits the BRAF gene, which encodes for B-raf protein, a proto-oncogene involved in various genetic mutations. This protein plays a role in regulating the MAP kinase/ERK signaling pathway, which impacts cell division, differentiation, and secretion. Mutations in this gene, most frequently the V600E mutation, are the most commonly identified cancer-causing mutations in melanoma, and have been isolated in various other cancers as well, including non-Hodgkin lymphoma, colorectal cancer, thyroid carcinoma, non-small cell lung carcinoma, hairy cell leukemia, and adenocarcinoma of the lung (DrugBank, https://go.drugbank.com/drugs/DB11718). On June 27, 2018, the Food and Drug Administration approved encorafenib and binimetinib (BRAFTOVI and MEKTOVI, Array BioPharma Inc.) in combination for patients with unresectable or metastatic melanoma with a BRAF V600E or V600K mutation, as detected by an FDA-approved test (PubChem, Kim et al., 2021). The systematic name (CAS Registry Number 1269440-17-6) is methyl *N*-[(2S)-1-[[4-[3-[5-chloro-2-fluoro-3-(methanesulfonamido) phenyl]-1-propan-2-ylpyrazol-4-yl]pyrimidin-2-yl]amino] propan-2-yl]carbamate. A two-dimensional molecular diagram is shown in Figure 1.

Encorafenib was claimed in US Patent 8,501,758 B2 (Huang et al., 2013; IRM and Novartis). The development of encorafenib and other protein kinase inhibitors is summarized in Koelblinger et al. (2018) and Imran et al. (2021). A European Medicines Agency (2018) report indicates that single-crystal and powder X-ray diffraction have been carried out on encorafenib, but we are unaware of any published X-ray diffraction data on this compound.

This work was carried out as part of a project (Kaduk et al., 2014) to determine the crystal structures of large-volume commercial pharmaceuticals, and include high-quality powder diffraction data for them in the Powder Diffraction File (Gates-Rector and Blanton, 2019).

II. EXPERIMENTAL

Encorafenib was a commercial reagent, purchased from TargetMol (Batch #145984), and was used as-received. The white powder was packed into a 1.5-mm diameter Kapton capillary and rotated during the measurement at ~50 Hz. The powder pattern was measured at 295 K at beamline 11-BM (Antao et al., 2008; Lee et al., 2008; Wang et al., 2008) of the Advanced Photon Source at Argonne National Laboratory using a wavelength of 0.458119(2) Å from 0.5 to 50° 2θ with a step size of 0.001° and a counting time of 0.1 s/step. The high-resolution powder diffraction data were collected using twelve silicon crystal analyzers that allow for high angular resolution, high precision, and accurate peak positions. A mixture of silicon (NIST SRM 640c) and alumina (NIST SRM 676a) standards (ratio Al_2O_3:Si = 2:1 by weight) was used to calibrate the instrument and refine the monochromatic wavelength used in the experiment.

The pattern was indexed initially using JADE Pro (MDI, 2022) on a high-quality primitive monoclinic unit cell with $a = 16.13558$, $b = 17.09344$, $c = 9.50639$ Å, $\beta = 90.02°$, $V =$

[a]Author to whom correspondence should be addressed. Electronic mail: kaduk@polycrystallography.com

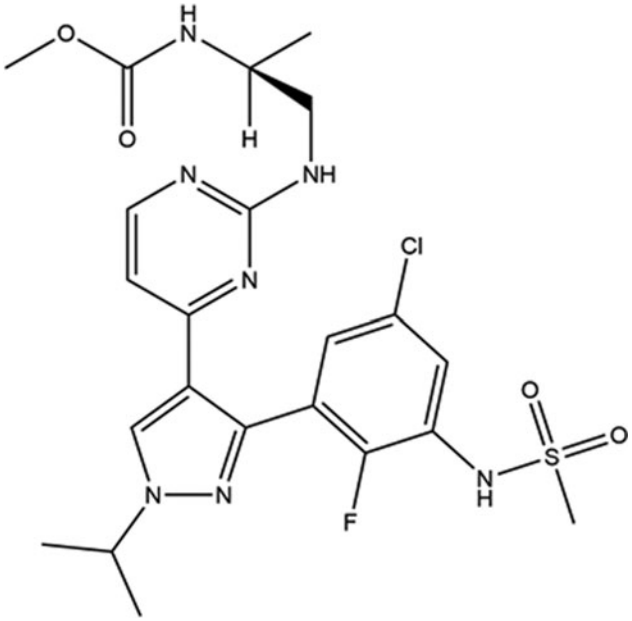

Figure 1. The 2D molecular structure of encorafenib.

2621.98 Å^3, and $Z = 4$. The β angle close to 90° suggested that the true symmetry might be orthorhombic. N-TREOR (Altomare et al., 2013) yielded an orthorhombic cell having similar dimensions, and suggested that the space group was $P22_12_1$. Attempts to solve the structure in this space group were unsuccessful, yielding molecular overlap and/or voids. A close examination of the pattern revealed that the 010 peak at 1.533° was present, though weak. Attempts to solve the structure in space group $P222_1$ were also unsuccessful, suggesting that the true space group was monoclinic $P2_1$, with an appropriate transformation of axes to yield the final cell with $a = 16.17355(25)$, $b = 9.52334(11)$, $c = 17.12368$ (19) Å, $\beta = 89.9928(22)°$, and $V = 2637.50(4)$ Å^3. This means that there are two independent encorafenib molecules in the asymmetric unit. Reduced cell searches of both the monoclinic and orthorhombic cells in the Cambridge Structural Database (Groom et al., 2016) with the chemistry C, H, Cl, F, N, O, and S only, yielded no hits.

An encorafenib molecule was downloaded from PubChem (Kim et al., 2021) as Conformer3D_CID_50922675.sdf. It was converted to a *.mol2 file using Mercury (Macrae et al., 2020). The structure was solved using Monte Carlo simulated annealing techniques as implemented in EXPO2014 (Altomare et al., 2013). After 6 days, only the best of the ten runs yielded a structure without molecular overlap.

The encorafenib unit cell does not account for the first two peaks in the pattern at 0.684 and 1.369° 2θ ($d = 38.396$ and 19.172 Å; Figure 2). These diffraction peaks apparently are the first- and second-order peaks from an additional unit cell having one long dimension. Initial refinements indicated the presence of two additional unindexed peaks, at $d = 4.1397$ and 3.7309 Å. Boolean searches of these two peaks in the Powder Diffraction File (Gates-Rector and Blanton, 2019) yielded hits similar to paraffin wax (or polyethylene), characteristic of the side-to-side packing of long paraffin chains. Adding the 39.4 Å peak to the searches yielded entry 02-092-6981, for heptadecanoic acid (CSD Refcode DARWAU01; Gbabode et al., 2007). This phase was added to the refinement to model these extra peaks, to avoid distorting the encorafenib structure to account for them. However, there is no evidence that heptadecanoic acid is actually present; this was merely a strategy to obtain a better refinement.

Rietveld refinement (begun from the VASP-optimized structure discussed below) was carried out using GSAS-II (Toby and Von Dreele, 2013). Only the 1.5–25.0° portion of the pattern was included in the refinement ($d_{min} = 1.058$ Å). All non-H bond distances and angles were subjected to restraints, based on a Mercury/Mogul Geometry check (Bruno et al., 2004; Sykes et al., 2011). The Mogul average and standard deviation for each quantity were used as the

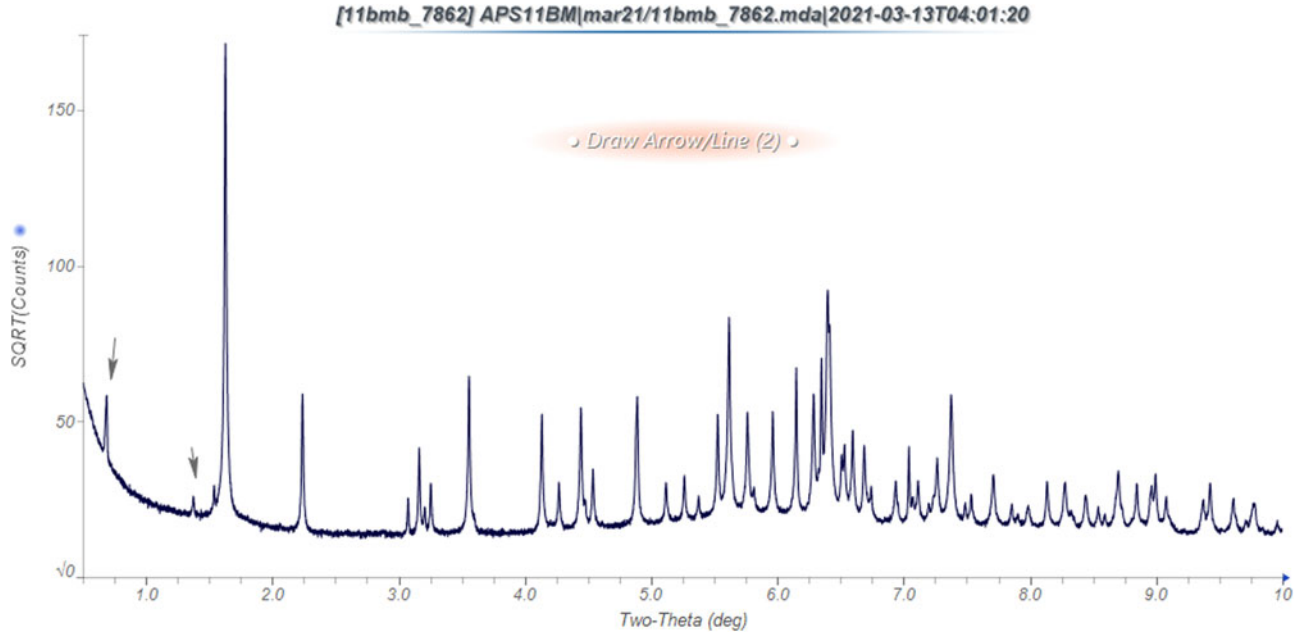

Figure 2. The synchrotron X-ray powder diffraction pattern of encorafenib indicates the two unindexed low-angle peaks. Note that the *y*-axis is a square root scale. Image generated using JADE Pro (MDI, 2022).

https://doi.org/10.1017/S0885715623000118 Published online by Cambridge University Press

restraint parameters. The restraints contributed 9.0% to the final χ^2. The hydrogen atoms were included in calculated positions, which were recalculated during the refinement using Materials Studio (Dassault Systèmes, 2021). The U_{iso} of the heavy atoms were grouped by chemical similarity. The U_{iso} for the H atoms were fixed at 1.3× the U_{iso} of the heavy atoms to which they are attached. The U_{iso} of a few atoms were refined to slightly negative values, so they were fixed at reasonable values. A 2nd-order spherical harmonic preferred orientation model was included in the refinement. The refined texture index was 1.023(1). The concentration of the impurity phase refined to 3.4(1) wt%. The peak profiles were described using the generalized microstrain model. The background was modeled using a 6-term shifted Chebyshev polynomial, and a broad peak at 6.14° 2θ to model the scattering from the Kapton capillary and any amorphous component.

The final refinement (begun from the result of the VASP calculation) of 249 variables using 23,538 observations and 186 restraints yielded the residuals $R_{wp} = 0.1237$ and GOF = 2.31. The largest peak (1.18 Å from C20) and hole (1.18 Å from C35) in the difference Fourier map were 0.43(10) and −0.43(10) eÅ^{-3}, respectively. The largest errors in the difference plot (Figure 3) are in the intensities of some of the low-angle encorafenib peaks. A Le Bail fit to the pattern yielded $R_{wp} = 0.0932$, so the Rietveld fit is acceptable.

The structure of encorafenib was optimized (fixed experimental unit cell) with density functional theory techniques using VASP (Kresse and Furthmüller, 1996) through the MedeA graphical interface (Materials Design, 2016). The calculations were carried out on 16 2.4 GHz processors (each with 4 GB RAM) of a 64-processor HP Proliant DL580 Generation 7 Linux cluster at North Central College. The calculation used the GGA-PBE functional, a plane wave cutoff energy of 400.0 eV, and a k-point spacing of 0.5 Å^{-1} leading to a 1 × 2 × 1 mesh, and took ∼74 h. A single-point density functional calculation (fixed experimental cell) and population analysis were carried out using CRYSTAL17 (Dovesi et al., 2018). The basis sets for the H, C, N, and O atoms in the calculation were those of Gatti et al. (1994), and those for Cl, F, and S were those of Peintinger et al. (2013). The calculations were run on a 3.5 GHz PC using 8 k-points and the B3LYP functional, and took ∼8.1 h.

III. RESULTS AND DISCUSSION

The root-mean-square (rms) Cartesian displacement between the Rietveld-refined and DFT-optimized structures of molecule 1 (the lower atom numbers) is 0.477 Å (Figure 4), and the maximum difference is 1.232 Å, at the methyl group C30. Other large displacements occur at the periphery of the molecule. The comparable quantities for molecule 2 are 0.622 and 2.020 Å, at the methyl group C83 (Figure 5). The orientation of the isopropyl group is significantly different in the refined and optimized structures. The agreement is outside the normal range for correct structures (van de Streek and Neumann, 2014). The number of refined parameters is large (∼250), so the refined structure may be less-accurate and less-precise than usual. The current structure is the most-reasonable one we have been able to obtain. The following discussion concentrates on the DFT-optimized structure. The asymmetric unit (with atom numbering) is illustrated in Figure 6. Some U_{iso} are larger than others, suggesting the possibility of disorder, especially in the side chains. Since the DFT optimization requires an ordered model, we concentrated on refining ordered models.

The best view of the crystal structure is down the short b-axis (Figure 7). The crystal structure consists of alternating layers of stacked halogenated phenyl rings and the other parts of the molecules perpendicular to the a-axis. The Miller indices of the mean planes of the phenyl rings are 1,9,−3 and 4,7,2. The mean planes of the pyrazine rings are 9,7,13 and −7,−5,11. The mean planes of the pyrimidine rings are 11,5,7 and −7,−4,9. The *Mercury* Aromatics Analyser

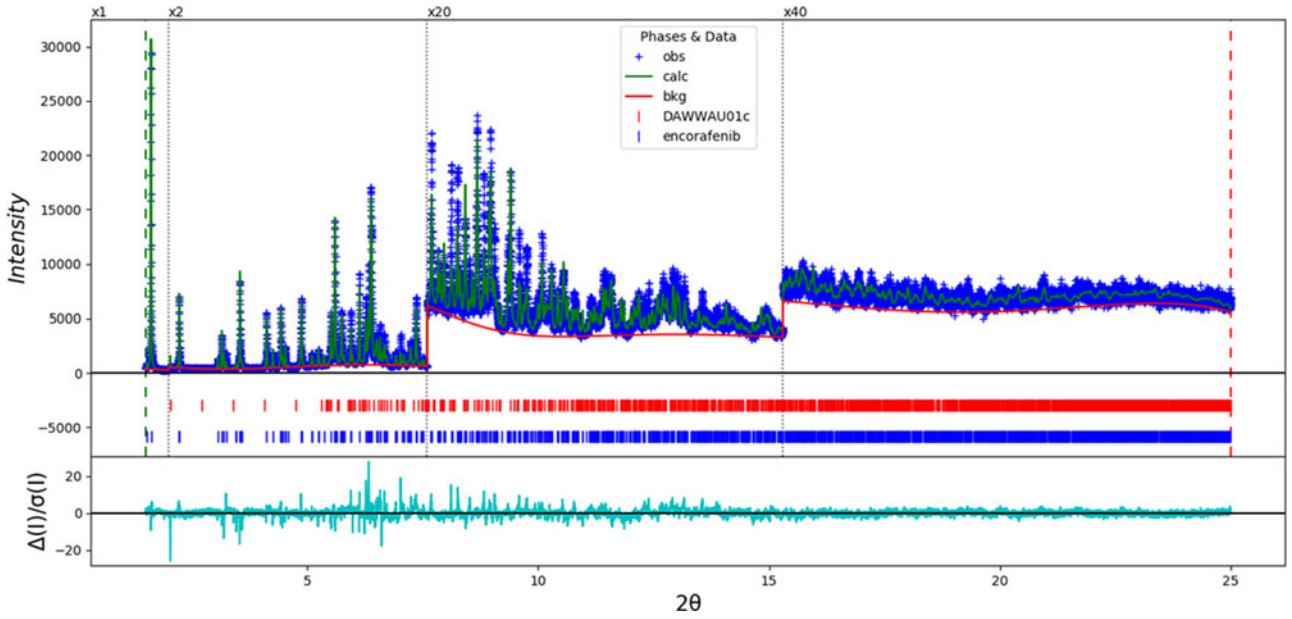

Figure 3. The Rietveld plot for the refinement of encorafenib. The blue crosses represent the observed data points, and the green line is the calculated pattern. The cyan curve is the normalized error plot, and the red line is the background curve. The vertical scale has been multiplied by a factor of 2× for 2θ > 2.0°, 20× for 2θ > 7.60°, and 40× for 2θ > 15.3°.

https://doi.org/10.1017/S0885715623000118 Published online by Cambridge University Press

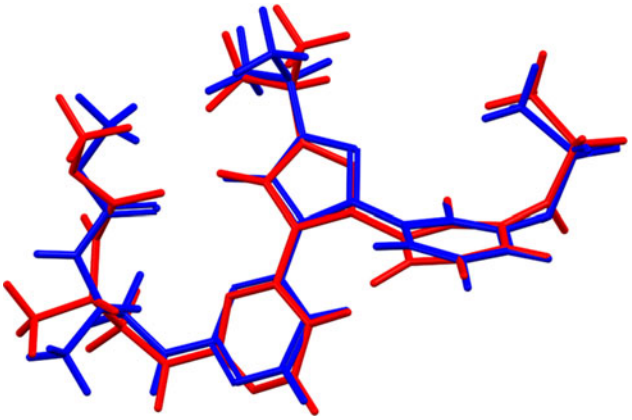

Figure 4. Comparison of the Rietveld-refined (red) and VASP-optimized (blue) structures of encorafenib molecule 1. The rms Cartesian displacement is 0.477 Å. Image generated using Mercury (Macrae et al., 2020).

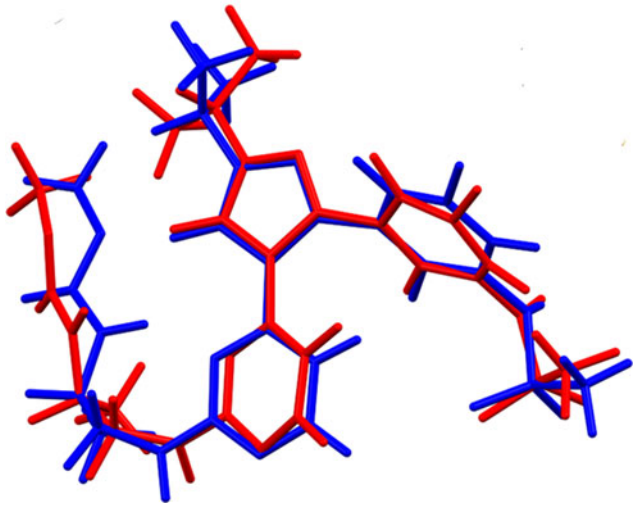

Figure 5. Comparison of the Rietveld-refined (red) and VASP-optimized (blue) structures of encorafenib molecule 2. The rms Cartesian displacement is 0.622 Å. Image generated using Mercury (Macrae et al., 2020).

indicates only one moderate interaction with a distance of 4.12 Å between the phenyl rings of molecules 1 and 2.

Almost all of the bond distances and bond angles fall within the normal ranges indicated by a Mercury/Mogul Geometry check (Macrae et al., 2020). The C2–N3 bond distance of 1.702 Å (average = 1.629(13) Å; *Z*-score = 5.6) is flagged as unusual. Occasionally bonds involving S are unusual in a VASP-optimized structure, so this characteristic may reflect the quality of the DFT calculation. The C24–N10–C28 angle of 117.6° (average = 123.9(16)°; *Z*-score 4.0) is flagged as unusual. Torsion angles involving rotations about the C15–N8, C16–C22, C17–C19, and C79–C85 bonds are flagged as unusual, but lie in low-frequency portions of broad distributions. Torsion angles involving rotation about the S65–N76, N73–C91, and C86–C87 bonds lie on the tails of bimodal distributions, so are slightly unusual. Torsion involving rotation about the C28–N10 and C23–C24 bonds is truly unusual. The conformation of the ester side chain of molecule 1 seems to be unusual, consistent with the large displacement coefficients in this portion of the molecule.

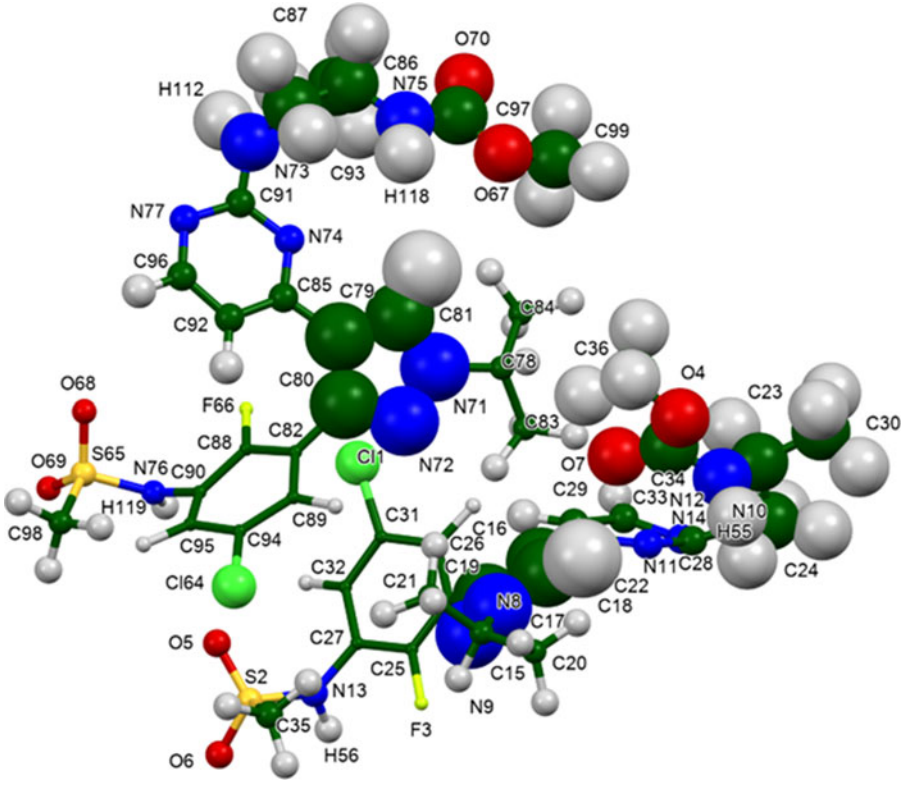

Figure 6. The asymmetric unit of encorafenib, with the atom numbering. The atoms are represented by 50% probability spheroids. Image generated using Mercury (Macrae et al., 2020).

https://doi.org/10.1017/S0885715623000118 Published online by Cambridge University Press

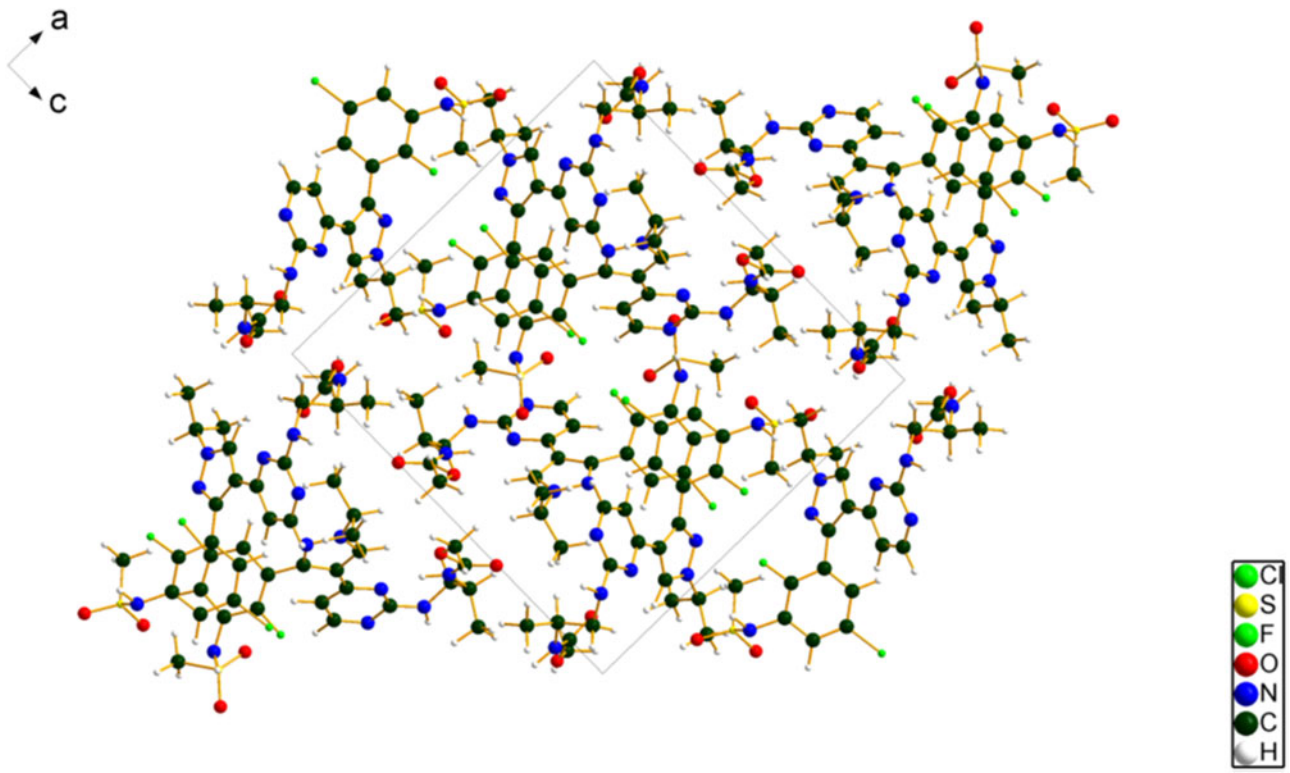

Figure 7. The crystal structure of encorafenib, viewed down the *b*-axis. Image generated using Diamond (Crystal Impact, 2022).

The two crystallographically independent molecules have similar overall shapes, but very different conformations (Figure 8). Quantum chemical geometry optimization of the isolated encorafenib molecules (DFT/B3LYP/6-31G*/water) using Spartan '18 (Wavefunction, 2020) indicated that the observed conformation of molecule 1 (lower atom numbers) is 0.3 kcal/mol lower in energy than that of molecule 2. The difference is well within the expected accuracy of such calculations, so the molecules should be considered equivalent in energy and the molecule is apparently flexible. A conformational analysis (MMFF force field) shows that the minimum-energy conformation is ~6 kcal/mol lower in

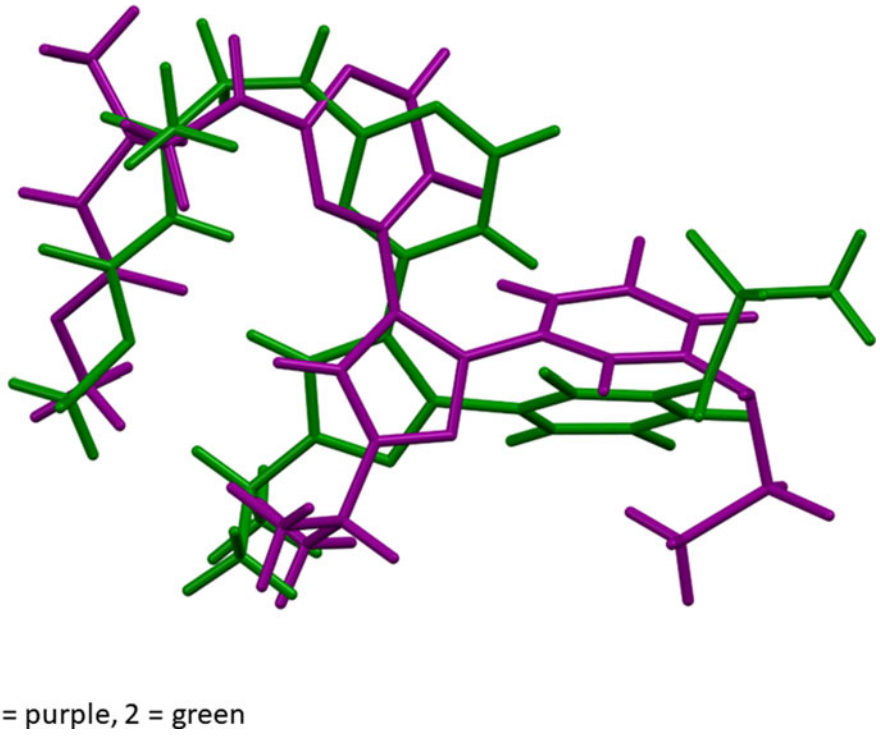

Figure 8. Comparison of the molecular structures of molecules 1 (purple) and 2 (green) in the crystal structure of encorafenib.

https://doi.org/10.1017/S0885715623000118 Published online by Cambridge University Press

TABLE I. Hydrogen bonds (CRYSTAL17) in encorafenib.

H-Bond	D-H (Å)	H···A (Å)	D···A (Å)	D-H···A (°)	Overlap (*e*)
N76–H119···N77	1.070	1.701	2.771	177.0	0.092
N75–H118···N74	1.032	2.041[a]	2.965	147.6	0.055
C96–H120···Cl1	1.090	2.983	3.951	148.1	0.010
C92–H113···C88	1.084	2.332[a]	3.201	136.1	0.010
C84–H107···O70	1.100	2.667	3.683	153.2	0.012
C81–H101···O67	1.082	2.335[a]	3.292	146.6	0.016
C36–H63···O6	1.094	2.337	3.153	129.9	0.014
C26–H18···N72	1.091	2.391	3.302	140.0	0.027
C24–H47···N11	1.095	2.427[a]	2.819	99.3	0.016
C23–H45···C28	1.102	2.632[a]	3.064	102.4	0.010
C18–H38···O7	1.084	2.476[a]	3.207	123.7	0.016

[a]Intramolecular.

energy, but contains a strong intramolecular N–H···O hydrogen bond (N12–H55···O5/6 or N73–H112···O68/69). An isolated encorafenib molecule thus folds on itself, showing that intermolecular interactions are important in determining the solid-state conformations.

Analysis of the contributions to the total crystal energy of the structure using the Forcite module of Materials Studio (Dassault Systèmes, 2021) suggests that angle and torsion distortion terms dominate the intramolecular deformation energy. The intermolecular energy is dominated by van der Waals and electrostatic attractions, which in this force field analysis also include hydrogen bonds. The hydrogen bonds are better analyzed using the results of the DFT calculation.

There are only a few hydrogen bonds in the structure (Table I), and the hydrogen bonding pattern is very different for the two molecules. Molecule 2 participates in two strong N–H···N hydrogen bonds (one intra- and the other intermolecular), which are not present for molecule 1. The intermolecular hydrogen bonds link molecule 2 into a spiral chain along the *b*-axis. The remaining hydrogen bonds are non-classical C–H···N; N/O/Cl links.

The volume enclosed by the Hirshfeld surface of the encorafenib asymmetric unit (Figure 9; Hirshfeld, 1977; Spackman et al., 2021) is 1307.44 Å^3, 99.14% of 1/2 the unit cell volume. The packing density is thus fairly typical. The volume of the Hirshfeld surface of molecule 1 (Figure 9(a)) is 648.23 Å^3, and that of molecule 2 (Figure 9(b)) is 652.81 Å^3; the sum of the individual volumes is 1301 Å^3. The only significant close contacts (red in Figure 9) involve the hydrogen bonds. The volume/non-hydrogen atom is typical, at 18.3 Å^3.

The Bravais–Friedel–Donnay–Harker (Bravais, 1866; Friedel, 1907; Donnay and Harker, 1937) morphology suggests that we might expect an elongated particle morphology for encorafenib, with 010 as the long axis. A 2nd-order spherical harmonic model was included in the refinement. The texture index was 1.023(1), indicating that preferred orientation was slight in this rotated capillary specimen.

IV. DEPOSITED DATA

The powder pattern of encorafenib from this synchrotron data set has been submitted to ICDD for inclusion in the Powder Diffraction File. The Crystallographic Information Framework (CIF) files containing the results of the Rietveld refinement (including the raw data) and the DFT geometry optimization were deposited with the ICDD. The data can be requested at pdj@icdd.com.

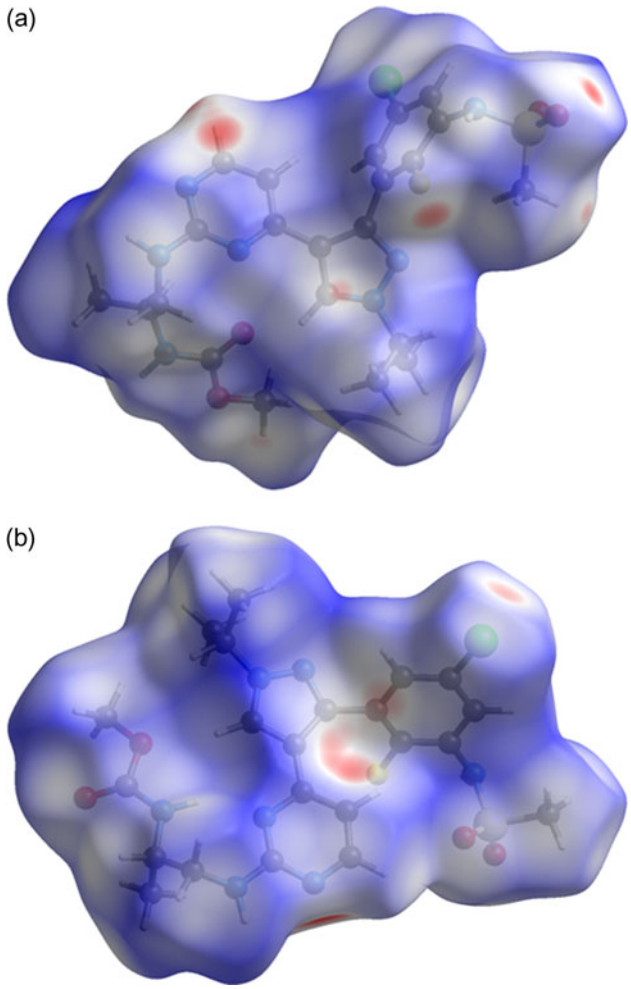

Figure 9. (a) The Hirshfeld surface of molecule 1 of encorafenib. Intermolecular contacts longer than the sums of the van der Waals radii are colored blue, and contacts shorter than the sums of the radii are colored red. Contacts equal to the sums of radii are white. Image generated using CrystalExplorer (Spackman et al., 2021). (b) The Hirshfeld surface of molecule 2 of encorafenib. Intermolecular contacts longer than the sums of the van der Waals radii are colored blue, and contacts shorter than the sums of the radii are colored red. Contacts equal to the sums of radii are white. Image generated using CrystalExplorer (Spackman et al., 2021).

ACKNOWLEDGEMENTS

The use of the Advanced Photon Source at Argonne National Laboratory was supported by the U.S. Department of Energy, Office of Science, Office of Basic Energy Sciences, under Contract No. DE-AC02-06CH11357. This work was partially supported by the International Centre for Diffraction Data. We thank Lynn Ribaud and Saul Lapidus for their assistance in the data collection.

CONFLICTS OF INTEREST

The authors have no conflicts of interest to declare.

https://doi.org/10.1017/S0885715623000118 Published online by Cambridge University Press

REFERENCES

Altomare, A., C. Cuocci, C. Giacovazzo, A. Moliterni, R. Rizzi, N. Corriero, and A. Falcicchio. 2013. "EXPO2013: A Kit of Tools for Phasing Crystal Structures from Powder Data." *Journal of Applied Crystallography* 46, 1231–1235.

Antao, S. M., I. Hassan, J. Wang, P. L. Lee, and B. H. Toby. 2008. "State-of-the-Art High-Resolution Powder X-Ray Diffraction (HRPXRD) Illustrated with Rietveld Refinement of Quartz, Sodalite, Tremolite, and Meionite." *Canadian Mineralogist* 46, 1501–1509.

Bravais, A. 1866. *Etudes Cristallographiques*. Gauthier Villars, Paris.

Bruno, I. J., J. C. Cole, M. Kessler, J. Luo, W. D. Sam Motherwell, L. H. Purkis, B. R. Smith, R. Taylor, R. I. Cooper, S. E. Harris, and A. Guy Orpen. 2004. "Retrieval of Crystallographically-Derived Molecular Geometry Information." *Journal of Chemical Information and Computer Sciences* 44, 2133–2144.

Crystal Impact. 2022. Diamond. V. 4.6.8. Crystal Impact - Dr. H. Putz & Dr. K. Brandenburg. Windows.

Dassault Systèmes. 2021. Materials Studio. V. 2021. BIOVIA. Windows.

Donnay, J. D. H., and D. Harker. 1937. "A New Law of Crystal Morphology Extending the Law of Bravais." *American Mineralogist* 22, 446–447.

Dovesi, R., A. Erba, R. Orlando, C. M. Zicovich-Wilson, B. Civalleri, L. Maschio, M. Rérat, S. Casassa, J. Baima, S. Salustro, and B. Kirtman. 2018. "Quantum-Mechanical Condensed Matter Simulations with CRYSTAL." *Wiley Interdisciplinary Reviews: Computational Molecular Science* 8, e1360.

European Medicines Agency. 2018. "Braftovi." Assessment Report EMA/CHMP/554696/2018.

Friedel, G. 1907. "Etudes sur la loi de Bravais." *Bulletin de Minéralogie* 30, 326–455.

Gates-Rector, S., and T. N. Blanton. 2019. "The Powder Diffraction File: A Quality Materials Characterization Database." *Powder Diffraction* 39, 352–360.

Gatti, C., V. R. Saunders, and C. Roetti. 1994. "Crystal-Field Effects on the Topological Properties of the Electron-Density in Molecular Crystals - the Case of Urea." *Journal of Chemical Physics* 101, 10686–10696.

Gbabode, G., P. Negrier, D. Mondieig, E. M. Calvo, T. Calvet, and M. À. Cuevas-Diarte. 2007. "Structures of the High-Temperature Solid Phases of the Odd-Numbered Fatty Acids from Tridecanoic Acid to Tricosanoic Acid." *Chemistry - A European Journal*, 3150–3159. doi:10.1002/chem.200600955.

Groom, C. R., I. J. Bruno, M. P. Lightfoot, and S. C. Ward. 2016. "The Cambridge Structural Database." *Acta Crystallographica Section B: Structural Science, Crystal Engineering and Materials* 72, 171–179.

Hirshfeld, F. L. 1977. "Bonded-Atom Fragments for Describing Molecular Charge Densities." *Theoretica Chemica Acta* 44, 129–138.

Huang, S., X. Jin, Z. Liu, D. Poon, J. Tellew, Y. Wan, X. Wang, and Y. Xie. 2013. "Compounds and Compositions as Protein Kinase Inhibitors." US Patent 8,501,758 B2.

Imran, M., S. M. Asdaq, S. A. Khan, D. Unnikrishnan Meenakshi, A. S. Alamri, W. F. Alsanie, M. Alhomrani, Y. Mohzari, A. Alrashed, M. AlMotairi, and E. H. Alkhaldi 2021. "Innovations and Patent Trends in the Development of USFDA Approved Protein Kinase Inhibitors in the Last Two Decades." *Pharmaceuticals* 14, 710.

Kaduk, J. A., C. E. Crowder, K. Zhong, T. G. Fawcett, and M. R. Suchomel. 2014. "Crystal Structure of Atomoxetine Hydrochloride (Strattera), $C_{17}H_{22}NOCl$." *Powder Diffraction* 29, 269–273.

Kim, S., J. Chen, T. Cheng, A. Gindulyte, J. He, S. He, Q. Li, B. A. Shoemaker, P. A. Thiessen, B. Yu, L. Zaslavsky, J. Zhang, and E. E. Bolton. 2021. "PubChem in 2021: New Data Content and Improved Web Interfaces." *Nucleic Acids Research*, D1388–D1395. doi:10.1093/nar/gkaa971.

Koelblinger, P., O. Thuerigen, and R. Dummer. 2018. "Development of Encorafenib for BRAF-Mutated Advanced Melanoma." *Current Opinion in Oncology* 30, 125–133.

Kresse, G., and J. Furthmüller. 1996. "Efficiency of Ab-Initio Total Energy Calculations for Metals and Semiconductors Using a Plane-Wave Basis Set." *Computational Materials Science* 6, 15–50.

Lee, P. L., D. Shu, M. Ramanathan, C. Preissner, J. Wang, M. A. Beno, R. B. Von Dreele, L. Ribaud, C. Kurtz, S. M. Antao, X. Jiao, and B. H. Toby. 2008. "A Twelve-Analyzer Detector System for High-Resolution Powder Diffraction." *Journal of Synchrotron Radiation* 15, 427–432.

Macrae, C. F., I. Sovago, S. J. Cottrell, P. T. A. Galek, P. McCabe, E. Pidcock, M. Platings, G. P. Shields, J. S. Stevens, M. Towler, and P. A. Wood. 2020. "*Mercury 4.0*: From Visualization to Design and Prediction." *Journal of Applied Crystallography* 53, 226–235.

Materials Data Inc (MDI). 2022. JADE Pro. V. 8.6. Materials Data Inc.

Materials Design. 2016. MedeA. V. 2.20.4. Windows.

Peintinger, M. F., D. V. Oliveira, and T. Bredow. 2013. "Consistent Gaussian Basis Sets of Triple-Zeta Valence with Polarization Quality for Solid-State Calculations." *Journal of Computational Chemistry* 34, 451–459.

Spackman, P. R., M. J. Turner, J. J. McKinnon, S. K. Wolff, D. J. Grimwood, D. Jayatilaka, and M. A. Spackman. 2021. "Crystalexplorer: A Program for Hirshfeld Surface Analysis, Visualization and Quantitative Analysis of Molecular Crystals." *Journal of Applied Crystallography*, 1006–1011. doi:10.1107/S1600576721002910.

Sykes, R. A., P. McCabe, F. H. Allen, G. M. Battle, I. J. Bruno, and P. A. Wood. 2011. "New Software for Statistical Analysis of Cambridge Structural Database Data." *Journal of Applied Crystallography* 44, 882–886.

Toby, B. H., and R. B. Von Dreele. 2013. "GSAS II: The Genesis of a Modern Open Source All Purpose Crystallography Software Package." *Journal of Applied Crystallography* 46: 544–549.

van de Streek, J., and M. A. Neumann. 2014. "Validation of Molecular Crystal Structures from Powder Diffraction Data with Dispersion-Corrected Density Functional Theory (DFT-D)." *Acta Crystallographica Section B: Structural Science, Crystal Engineering and Materials* 70, 1020–1032.

Wang, J., B. H. Toby, P. L. Lee, L. Ribaud, S. M. Antao, C. Kurtz, M. Ramanathan, R. B. Von Dreele, and M. A. Beno. 2008. "A Dedicated Powder Diffraction Beamline at the Advanced Photon Source: Commissioning and Early Operational Results." *Review of Scientific Instruments* 79, 085105.

Wavefunction, Inc. 2020. Spartan '18. V. 1.4.5. Wavefunction Inc, Irvine, CA.

https://doi.org/10.1017/S0885715623000118 Published online by Cambridge University Press